
Supercharging Imbalanced Data Learning With Energy-based Contrastive Representation Transfer

Zidi Xiu* Junya Chen* Benjamin Goldstein Ricardo Henao Lawrence Carin

Chenyang Tao[†]

Duke University

{zidi.xiu, junya.chen, chenyang.tao}@duke.edu

Abstract

Dealing with severe class imbalance poses a major challenge for many real-world applications, especially when the accurate classification and generalization of minority classes are of primary interest. In computer vision and NLP, learning from datasets with long-tail behavior is a recurring theme, especially for naturally occurring labels. Existing solutions mostly appeal to sampling or weighting adjustments to alleviate the extreme imbalance, or impose inductive bias to prioritize generalizable associations. Here we take a novel perspective to promote sample efficiency and model generalization based on the invariance principles of causality. Our contribution posits a meta-distributional scenario, where the causal generating mechanism for label-conditional features is invariant across different labels. Such causal assumption enables efficient knowledge transfer from the dominant classes to their under-represented counterparts, even if their feature distributions show apparent disparities. This allows us to leverage a causal data augmentation procedure to enlarge the representation of minority classes. Our development is orthogonal to the existing imbalanced data learning techniques thus can be seamlessly integrated. The proposed approach is validated on an extensive set of synthetic and real-world tasks against state-of-the-art solutions.

1 Introduction

Learning with imbalanced datasets is a common yet still very challenging scenario in many machine learning applications. Typical scenarios include: *(i)* rare events, where the event prevalence is extremely low while their implications are of high cost, *e.g.*, severe risks that people seek to avert [56]; *(ii)* emerging objects in a dynamic environment, which call for quick adaptation of an agent to identify new cases with only a handful target examples and plentiful past experience [31]. A typical scenario in natural datasets is that the occurrence of different objects follows a power law distribution. And in many situations, the accurate identification of those rarer instances bears more significant social-economic values, *e.g.*, fraud detection [24], driving safety [27], nature conservation [50], social fairness [17], and public health [63, 92].

Notably, severe class imbalance and lack of minority labels are the two major difficulties in this setting, which render standard learning strategies unsuitable [57]. Without explicit statistical adjustments, the imbalance induces bias towards the majority classes. On the other hand, the lack of minority representations prevents the identification of stable correlations that generalize in predictive settings. In addition, due to technological advancements, more and higher dimensional data are routinely collected for analysis. This also inadvertently exacerbates the issue of minority modeling as there is an excess of predictors relative to the limited occurrence of minority samples.

*Contributed equally.

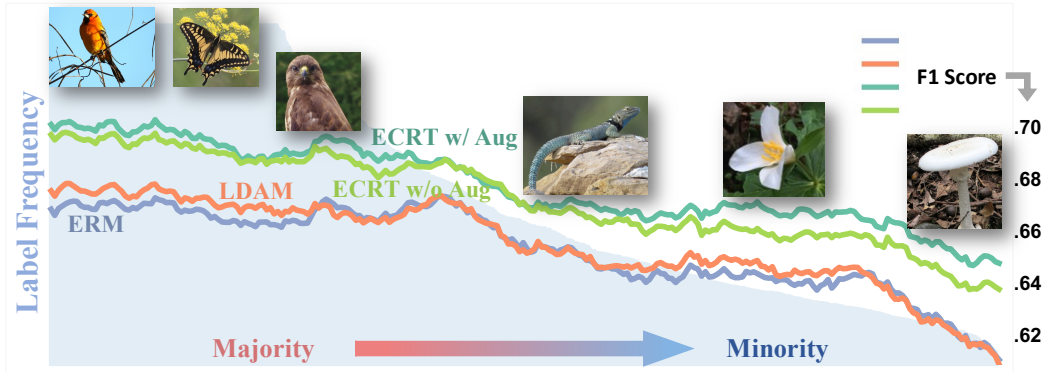


Figure 1: Energy-based causal representation transfer alleviates tail imbalance for natural image classification. The shaded region denotes label frequency in the iNaturalist data, with some representative images shown. Solid curves are for label-conditional F1 scores (higher is better) for the proposed *energy-based causal representation transfer* (ECRT), LDAM (state of the art) and the standard ERM. ECRT consistently outperforms the others, especially in the low-sample regime.

Various research efforts have been directed to address the above issues, with class re-balancing being the most popular heuristic. The two most prominent directions in the category include statistical *resampling* and *reweighting*. Resampling alters the exposure frequency during training, *i.e.*, more for the minorities and less so for the majorities [29]. Alternatively, reweighting directly amends the relative importance of each sample based on their class [22], sampling frequency [7] and associated cost for misclassification [30]. Recent developments also have considered class-sensitive and data-adaptive losses to more flexibly offset the imbalance [10, 60, 65, 55, 80, 51]. While being intuitive and working reasonably well in practice, an important is that these approaches offer no protection against the over-fitting of minority instances (see Figure 1)[91], a fundamental obstacle towards better generalization.

To circumvent this key limitation, inductive biases are often solicited to impose strong constraints that suppress spurious correlations that hinder out-of-sample generalization. A classical strategy is few-shot learning [31, 89, 40], where the majority examples are used to train meta-predictors and transferable features, leaving only a few parameters to tune for the minority data. In anomaly detection, methods such as one-class classification instead regard minority classes as outliers that do not always associate with stable, recognizable patterns [67, 75].

Despite their relatively strong assumptions, these methods capitalize on their superior ability in generalizing in the low sample regime in empirical settings.

More recently, establishing causal invariance has emerged as a new, powerful learning principle for better generalization ability even under apparent distribution shifts [73]. In contrast to standard empirical risk minimization (ERM) schemes, where the generalization to similar data distributions is considered, causally-inspired learning instead embraces robustness against potential perturbations [5]. This is achieved via only attending to causally relevant features and associations postulated to be invariant under different settings [70]. Specifically, contributions from spurious, unstable features are effectively blocked or attenuated. Interestingly, compromise of performance can be expected in those models [74], as a direct consequence of discarding useful (but non-causal) correlations in exchange for better causal generalization. Recently, [48] proposed non-parametric causal disentanglement of data representation to identify invariant relations.

This work explores the advancement of imbalanced data learning via adopting causal perspectives, with the insight that the key algorithm can be reformulated as an energy-based contrastive learning procedure to drastically improve efficiency and flexibility. In recognition of the limitations discussed above, we present *energy-based causal representation transfer* (ECRT): a novel imbalanced learning scheme that brings together ideas from causality, contrastive learning, energy modeling, data-augmentation and weakly-supervised learning, to address the identified weakness of existing solutions. Our key contributions are: (i) a causal representation encoder informed by an invariant generative mechanism based on generalized contrastive learning; (ii) integrated data-augmentation and source representation regularization techniques exploiting feature independence to enrich mi-

nority representations that better balance the trade-off between utility and invariance; (iii) a key novelty is the derivation of an energy-based contrastive learning algorithm that greatly enhance model parallelism for large-label settings and extends generalized contrastive learning; and (iv) insightful discussions on the justifications for the use of the proposed approach. Our claims are supported by strong experimental evidence.

2 Preliminaries

Notation and problem definition. We use $x \in \mathbb{R}^p$ to denote the input data and $z \in \mathbb{R}^d$ for the predictive features extracted from x . Let $y \in \{1, \dots, M\}$ be the class label. The number of training samples and those with label m are denoted as n and n_m , respectively. We use $\mathbb{E}[\cdot]$ to denote the expectation (average) of an empirical distribution, \mathbf{a}_i to denote a vector associated with the i -th sample, and $[\mathbf{a}]_b$ to denote the b -th entry of vector \mathbf{a} . For simplicity, we assume class M is the minority class, i.e., $n_m \gg n_M$, for $m \in \{1, \dots, M-1\}$. Throughout, we refer to \mathcal{X} , \mathcal{Z} and \mathcal{S} as data, feature, and source spaces, respectively, as shown in Figure 2, and defined below. Our goal is to accurately predict the label of minority instances with very limited training examples of it. Generalization to multiple minority categories is straightforward.

Generalized contrastive learning and ICA The proposed approach is based on a generalized form of *independent component analysis* (ICA), which addresses the inverse problem of signal *disentanglement* [46]. Specifically, ICA decorrelates features \mathbf{Z} of the observed signal \mathbf{X} into a source signal representation $\mathbf{S} = f_\psi(\mathbf{Z})$, where $f_\psi(z)$ is a smooth and invertible mapping known as the *de-mixing* function, and while assuming that the components of \mathbf{S} are statistically independent, i.e., with density $q(\mathbf{s}) = \prod_j q_j([\mathbf{s}]_j)$. Notationally, we call $[\mathbf{s}]_j$ the j -th *independent component* (IC) of \mathbf{Z} . While *nonlinear ICA* (NICA) is generally infeasible [19, 47], [48] has recently proposed a setting in which the identification of NICA can be achieved, by requiring an additional auxiliary label y . Specifically, NICA assumes that source signals are conditionally independent given y , i.e., $q(\mathbf{s}|y) = \prod_j q_j([\mathbf{s}]_j|y)$, then $f_\psi(z)$ can be identified using *generalized contrastive learning* (GCL), whose implementation is detailed below.

GCL solves a generalized regression problem in which a *critic function* predicts whether label y and representation \mathbf{z} are correctly paired, i.e., *congruent*. We call (y_i, \mathbf{z}_i) a congruent pair and (y_j, \mathbf{z}_j) an incongruent pair if $i \neq j$. Specifically, the critic is defined as $r_\nu(y, \mathbf{z}) = \sum_{a=1}^d r_\nu^a(y, [\mathbf{s}]_a)$, where $r_\nu^a(\cdot, \cdot)$ is a neural network with parameters ν , whose inputs are the label y and the a -th coordinate of $\mathbf{s} = f_\psi(\mathbf{z})$, denoted as $[\mathbf{s}]_a$. Then, GCL optimizes the following objective:

$$\arg \min_{f_\psi, r_\nu} \underbrace{\mathbb{E}_i[h(-r_\nu(y_i, \mathbf{z}_i))] + \mathbb{E}_{j \neq i}[h(r_\nu(y_j, \mathbf{z}_i))]}_{\mathcal{L}_{\text{GCL}}(f_\psi, r_\nu)}, \quad (1)$$

where $h(r) = \log(1 + \exp(r))$ is the softplus function. (1) seeks to optimize $f_\psi(\cdot)$ and $r_\nu(\cdot, \cdot)$ by maximizing the discriminative power to tell apart congruent and incongruent pairs.

In fact, an interesting result showed by [48] revealed that maximizing the ability of the critic function $r_\nu(\cdot, \cdot)$ for correctly identifying matching pairs (\mathbf{z}, y) leads to the identification (up to univariate transformation) of $f_\psi(\cdot)$, such that the components of \mathbf{s} are conditionally independent given y . See the Supplementary Material (SM) for a formal exposition.

3 Energy-based Causal Representation Transfer

In this section, we describe the construction of *energy-based causal representation transfer* (ECRT): a causally informed data transformation and augmentation procedure to improve learning with imbalanced datasets. Our model assumes a shared causal data-generation procedure, which can be accurately identified by learning with the majority classes under assumed class-conditional representation independence. We obtain decorrelated representations that facilitate data augmentation and efficient learning with minority classes.

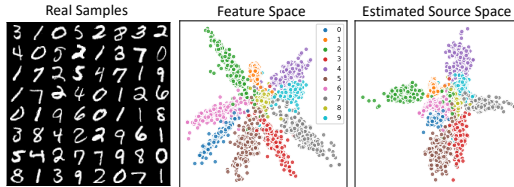


Figure 2: Illustration of data space \mathcal{X} , feature space \mathcal{Z} (predictive but entangled) and source space \mathcal{S} (independent, or disentangled) representations identified by ECRT for MNIST.

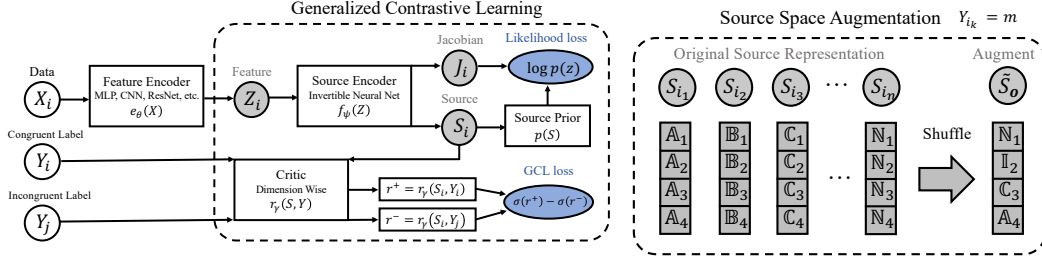


Figure 3: Source space estimation module of ECRT. We use GCL to identify the demixing function $s = f_\psi(z)$ via telling apart congruent & incongruent pairs.

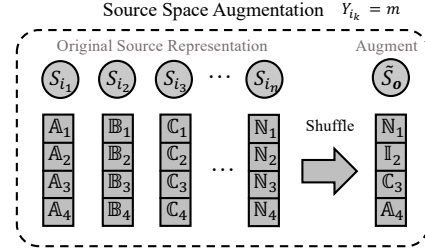


Figure 4: Non-parametric source space augmentation based on shuffling.

The proposed model consists of the following components: (i) a feature encoder module $z = e_\theta(x)$; (ii) two classification modules, $h_{\phi'}(z)$ and $h_\phi(s)$, for predicting label y from features z and sources s , respectively; (iii) a nonlinear ICA module for the de-mixing function $s = f_\psi(z)$; (iv) a critic function $r_\nu(y, z)$ for GCL; and (v) a data augmentation module. Further, $(\theta, \phi', \phi, \psi, \nu)$ denote the parameters of all the neural-network-based modules. Algorithm 1 outlines a general workflow, and below, we elaborate on our assumptions and detail the implementation of ECRT.

3.1 Model assumptions

To enable knowledge transfer across classes, we make the following assumptions:

Assumption 3.1. Let z be a sufficient statistic (features) of x for predicting label y , all class conditional feature distributions $p(z|y)$ share a common ICA demixing function $f_\psi(z)$.

This implies there exists a smooth invertible function $f_\psi : \mathcal{Z} \rightarrow \mathcal{S}$, and a set of IC distributions $\{q(s|y = m)\}_{m=1}^M$, that are linked to the conditional feature distributions $p(z|y = m)$ via $S^m = f_\psi(Z^m)$, where $S^m \sim q(s|y = m)$ and $Z^m \sim p(z|y = m)$. The subscript m in S^m and Z^m indicates $y = m$, in a slight abuse of notation.

Importantly, $f_\psi^{-1}(s) : \mathcal{S} \rightarrow \mathcal{Z}$ is the *invariant causal mechanism* underlying the features of observed data. This specification, which is consistent with Assumption 3.1 enables the identification of the shared generating process, namely, the de-mixing function $f_\psi(z)$ that connects the likely dissimilar conditionals $\{p(z|y = m)\}_{m=1}^M$ via the source conditionals $\{q(s|y = m)\}_{m=1}^M$, as demonstrated in the context of NICA by [48]

A shortcoming of Assumption 3.1 is that the hypothesis supporting it is somewhat strong, untestable and may not hold in practice. However, we argue that the structural constraints imposed on the model by the assumption via the source conditionals $q(s|y = m)$ and the invertibility of $f_\psi(z)$, restrict the search space of the otherwise over-flexible model space powered by neural networks. Further, the causal mechanism implied by $f_\psi^{-1}(s)$ enables an effective knowledge transfer mechanism across classes via $q(s|y = m)$.

3.2 Energy-based Causal Representation Transfer

Encoder pre-training. To implement ECRT, we first find a good (reduced) feature representation of x highly predictive of label y . This can be achieved via supervised representation learning (see Figure 3), which optimizes an encoder and predictor pair $(e_\theta(x), h_{\phi'}(z))$ to minimize the label prediction risk $\mathcal{L}(\phi') \triangleq \mathbb{E}[\ell(h_{\phi'}(e_\theta(x)), y)]$, where $\ell(\cdot, \cdot)$ is a suitable loss function, e.g., cross-entropy, hinge loss, etc. To avoid capturing *spurious* (non-generalizable) features that overfit the minority class, we advocate training only with majority samples at this stage; assuming that $M > 2$. Alternatively, one could also consider unsupervised feature extraction schemes, such as auto-encoders. Further, we also recommend using statistical adjustments such as importance weighting, to reduce the impact of data imbalance.

De-mixing representation with GCL. After obtaining a good feature representation $\mathbf{Z} = e_\theta(\mathbf{X})$, we proceed to learn the de-mixing function $f_\psi(\mathbf{z})$, such that the coordinates of the source representation $\mathbf{S} = f_\psi(\mathbf{Z})$ are (approximately) independent given the label y . This can be done by optimizing the GCL objective in (1) with respect to the feature representation and label pairings (y, \mathbf{z}) , adopting the *masked auto-regressive flow* (MAF) [69] to model the smooth, invertible transformation $f_\psi(\mathbf{z})$, which allows efficient parallelization of the autoregressive architecture via *causal masking* [14]. The procedure is outlined in Figure 3.

Augmenting the minority. Inspired by [83], we artificially augment the minority feature representations \mathbf{z} via random permutations in the source space \mathcal{S} , as shown in Figure 4. Provided the assumed conditional independence of the sources, the features \mathbf{Z}^m corresponding to label $y = m$ are generated by $\mathbf{Z}^m = f_\psi^{-1}(\mathbf{S}^m)$, where each dimension in the source representation $[\mathbf{S}^m]_j \sim q([s]_j | y = m)$ are independently and *implicitly* sampled as described below. Specifically, using the (estimated) de-mixing function $f_\psi(\mathbf{z})$, we can obtain an approximate empirical source distribution for each $y = m$, i.e., $S^m \triangleq \{s_i = f_\psi(e_\theta(\mathbf{x}_i)) | y_i = m\} = \{s_i\}_{i=1}^{n_m}$, where S^m is a collection of n_m samples of $q(s | y = m)$. Then, we can draw new artificial samples $\tilde{s}^m \sim q(s | y = m)$ by randomly permuting the coordinates within elements S^m independently via

$$\tilde{s}_o^m = ([s_{o_1}^m]_1, [s_{o_2}^m]_2, \dots, [s_{o_d}^m]_d), \quad (2)$$

where $o = (o_1, \dots, o_d)$ is a random permutation of $(1, \dots, n_m)$. Note we have used \tilde{s}_o^m to emphasize that the source point is artificially created via permutation o . We call this procedure *nonparametric augmentation* because it does not make distributional assumptions for $q(s | y = m)$. However, below we will discuss its limitations and consider an alternative where a parametric form is assumed. While it is tempting to refine the predictor $h_{\phi'}(\mathbf{z})$ with artificial features augmented via $\tilde{\mathbf{z}}^m = f_\psi^{-1}(\tilde{s}^m)$, in Section 3.3 we will argue that it stands to benefit more from training a new predictor directly based on source representations, i.e., $h_\phi(\mathbf{s})$, without the need for inverting $f_\psi(\mathbf{z})$.

Model refinement. Now we can leverage the augmented data to refine the prediction model. For minority class $y = M$, we optimize the following objective

$$\mathcal{L}_{\text{AUG}}(\phi') = \mathcal{L}(\phi') + \lambda(\mathbb{E}_{\tilde{\mathbf{Z}}^M}[\ell(h_{\phi'}(\tilde{\mathbf{z}}^M), M)] - \mathbb{E}_{\mathbf{Z}^M}[\ell(h_{\phi'}(\mathbf{z}), M)]), \quad (3)$$

where $\mathcal{L}(\phi')$ is the loss used for pre-training. Conceptually, (3) replaces a portion of the minority samples with augmentations. The trade-off parameter $\lambda \in [0, 1]$ encodes the relative confidence for trusting the artificially generated representations $\tilde{\mathbf{Z}}^M$ obtained from S^M for the minority label $y = M$. Further, at this stage we found it's beneficial to fix the encoder module to prevent the de-mixing function to accommodate the changes in the encoder which in practice may cause instability during training.

Challenges with naïve implementation. We identify three major issues with naïvely implemented ECRT, to be addressed in the section below: (i) *Representation conflict*: since the GCL solution is not unique, we do observe naïve GCL training drifts among viable source representations whose performance differ considerably, causing stability concerns; (ii) *Costly augmentation*: MAF inversions dominate the computation load during training, which becomes prohibitive in high dimensions; and (iii) *Gridding artifact*: a small minority sample size leads to pronounced augmentation bias when sampling nonparametrically via (2), manifested as a rectangular-shaped grid (see Figure 5).

3.3 Improving causal representation transfer

Energy-based GCL. Our key insight to improve GCL comes from the fact that Equation (1) is essentially learning the density ratio between the joint and product of marginals, i.e., $\frac{p(\mathbf{x}, \mathbf{y})}{p(\mathbf{x})p(\mathbf{y})}$. This immediately reminds us the recent literature on contrastive *mutual information* (MI) estimators, such as InfoNCE [71]. In such works, a variational lower bound of MI is derived, and the algorithm optimizes a critic function using the positive samples from the joint distribution, and the negative samples from the product of the marginals. At their optimal value, these critics recover the density ratio or a transformation of it. Our development is based on the recent work of [37], using an energy-perspective to improve contrastive learning. Specifically, we will be using a variant of the celebrated *Donsker-Varadhan* (DV) estimator [28], and applied Fenchel duality trick to compute a solution [32, 81, 23]. Specifically, the *Fenchel-Donsker-Varadhan* (FDV) estimator takes the following form:

$$I_{\text{FDV}} \triangleq \hat{I}_{\text{DV}}^K(\{\mathbf{x}_i, \mathbf{y}_i\}) + \frac{\sum_j \exp[(g_\theta(\mathbf{x}_i, \mathbf{y}_j) - g_\theta(\mathbf{x}_i, \mathbf{y}_i))/\tau]}{\sum_j \exp[(\hat{g}_\theta(\mathbf{x}_i, \mathbf{y}_j) - \hat{g}_\theta(\mathbf{x}_i, \mathbf{y}_i))/\tau]} + 1, \quad (4)$$

where $g_\theta(\mathbf{x}_i, \mathbf{y}_i)$ is our critic of interest and $\hat{I}_{\text{DV}}^K(\{\mathbf{x}_k, \mathbf{y}_k\}) = g(\mathbf{x}_1, \mathbf{y}_1) - \log(\sum_{k'=1}^K \exp(g(\mathbf{x}_1, \mathbf{y}'_{k'}))/K)$ is the *Donsker-Varadhan* (DV) estimator [28] for the MI. Using the same parameterization used in GCL recovers the same causal identification property (see Appendix for details). Compared to the original GCL formulation, we are now using multiple negative samples instead of one, which greatly boosts learning efficiency [38]. And this can be efficiently implemented with the *bilinear* critic trick [15, 13, 37] so that all in-batch data can be used as negatives. In our context, it greatly boosts training efficiency when dealing with a large number of different classes. See Algorithm S1 in Appendix.

Regularizing the data likelihood. Recall GCL solutions can only be identified up to an invertible transformation of each dimension [48], and the predictive performance of different valid GCL solutions can vary significantly. Empirically, we observe that a naive implementation of GCL often leads to source representations that are densely packed (see Figure S1 in the SM). This is undesirable, when decoding back to the feature space and making useful predictions, the neural network predictor will need to be expansive, *i.e.*, requiring a large Lipschitz constant, thereby sacrificing optimization stability and model generalization according to existing learning theory [20, 87].

To encourage source representations that are less condensed, we consider a simple, intuitive strategy consisting of regularizing the source representation with the log-likelihood in feature space. This likelihood can be easily obtained with MAF using $\ell_{\text{FLOW}}(f_\psi)$ defined in the SM. Following common practice, we set source prior $p(\mathbf{s})$ to the standard Gaussian, and optimize the following likelihood-regularized GCL objective:

$$\tilde{\mathcal{L}}_{\text{GCL}}(f_\psi, r_\nu) = \mathcal{L}_{\text{GCL}}(f_\psi, r_\nu) + \rho \mathcal{L}_{\text{FLOW}}(f_\psi), \quad (5)$$

where $\rho > 0$ is the regularization strength. Naturally, this regularization will encourage the global source representation identified by GCL to be more consistent with a Gaussian-shaped distribution.

An alternative interpretation for the likelihood-regularized objective in (5) is that it can be understood as a relaxation to the conditional independence (Assumption 3.1). To see this, recall the likelihood objective obtained from the *invertible neural networks* (INN) alone attempts to map the source representations to be *unconditionally* independent, as opposed to the *conditional* independence assumed by

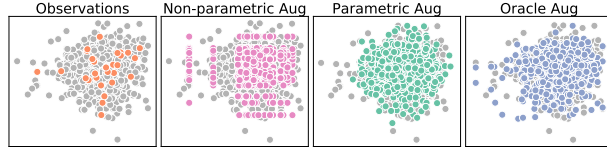


Figure 5: Comparison of different source augmentations overlaid on the ground-truth distribution (gray dots). A severe *gridding artifact* is observed in the low-sample regime for the nonparametric scheme, whereas the parametric augmentation closely matches the oracle in distribution.

NICA. The regularized formulation (5) provides a safe “*fall-back*” mode in case Assumption 3.1 is violated. This also motivates us to consider an important variant: making multiple class-dependent source priors, *i.e.*, $p^m(\mathbf{s})$ for each class label $m \in \{1, \dots, M\}$ in (5), whose parameters (*i.e.*, mean and variance) are jointly learned with other model parameters. Compared to the fully non-parametric objective (1), this strategy further encourages the source representations to be independent given the class labels, and it enables *parametric* data augmentation, *i.e.*, sampling from the parametric label priors instead of permuting the indices. We refer to this variant as ECRT-MP, where MP stands for multiple priors. And similarly, ECRT-IP refers to the case when a single prior is used. We have found that ECRT-MP performs better in most cases, and consequently, ECRT means ECRT-MP by default.

Modeling in the source space. Rather than modeling the predictor $h_{\phi'}(\mathbf{z})$ in the feature space \mathcal{Z} , we advocate instead for building the predictor directly in the source space \mathcal{S} , *i.e.*, modeling with $h_\phi(\mathbf{s})$. This practice enjoys several benefits: (i) *Easy & robust augmentation*: many designs of high-dimensional flows are asymmetric computationally, and inverting a MAF is not only d times more costly than a forward pass, it is also numerically unstable at the boundary. Direct modeling in the source space circumvents the difficulties associated with MAF inversions during data augmentation; (ii) *Feature whitening*: the source representation identified by GCL is component-wise independent, and literature documents abundant empirical evidence that similar de-correlation based pre-processing, commonly known as *whitening*, benefits learning [45, 6, 49].

Parametric augmentation. When the number of minority observations is scarce, the above non-parametric indices-shuffling augmentation suffers from the *gridding artifact* (Figure 5). This artifact amplifies the augmentation bias in the low-sample regime. To overcome this limitation, we empirically observe that the estimated class-conditional source distributions are usually Gaussian-like after the

likelihood regularization (especially so when label conditional priors are used). In these situations, a parametric augmentation that draws synthetic source samples from a Gaussian distribution matched to the empirical mean and variance of minority source representations is more efficient.

3.4 Insights and remarks

To better appreciate the gains and limitations expected from ECRT, we compile a few complementary arguments below, through the lens of very different perspectives.

Why causal augmentation works. It is helpful to understand the gains from ECRT’s causal augmentation beyond the heuristic that permuting the ICs provides more training samples for the minority class. [83] considered a similar causal augmentation procedure for few-shot learning, and provided two major theoretical arguments: (i) the risk estimator based on the augmented examples is the uniformly minimum variance unbiased estimator given the accurate estimation of f_ψ (see Theorem 1, [83]); and (ii) with high probability, the generalization gap can be bounded by the approximation error of f_ψ (see Theorem 2, [83]). In the SM, we give arguments that our causal augments give the ‘best’ label-conditional distribution estimate.

Speedup from shared embedding. While for typical supervised learning tasks the generalization bound scale as $\mathcal{O}(n^{-\frac{1}{2}})$, a superior rate of $\mathcal{O}(n^{-\eta})$ where $\eta \in [\frac{1}{2}, 1]$ is possible, if there exists abundant data for an alternative, yet related task that shares the same feature embedding (see Theorem 3, [72]). Note n refers to the size of labeled data directly related to the *strong* task of interest, in our case, prediction of minority labels. Our ECRT employs GCL to identify one such common embedding, *i.e.*, the source space, using the majority examples, and consequently, improves predictions on the minority class.

Representation whitening. Our ECRT causally disentangles representation [78, 84] via de-correlating the representations conditionally. Extensive empirical evidence has pointed to the fact that such representation de-correlation, more commonly known as data whitening [52], is expected to considerably improve learning efficiency [18]. This benefit has been attributed to the better conditioning of the Fisher information matrix for gradient-based optimization [25], thus rectifying second-order curvatures to accelerate convergence. Our source space modeling explicitly separates the task of representation disentanglement, and in turn, helps the prediction network to focus on its primary goal.

Potential limitations. The setting considered by ECRT is restrictive in that it precludes the learning of useful, yet non-transferable features predictive of the minority labels. For instance, there might be a feature unique to the minority class. However, since the de-mixer $f_\psi(\mathbf{z})$ is only trained on the majority domains absent of this feature, it can not be accounted for by the ECRT model. This is a key limitation of causally inspired models, in that they are often too conservative for only retaining the invariant features, promoting cross-domain generalization at the cost of within-domain performance degradation [74].

4 Related Work

Causal invariance and representation learning. A major school of considerations for building robust machine learning models is to stipulate invariant causal relations across environments [76, 62, 12], such that one hopes to safely extrapolate beyond the training scenario [8]. We broadly categorize such efforts into two streams, namely predictive causal models and generative causal models. Prominent examples from the first category include ICP [70, 43] and IRM [5], which highlight the identification of invariant representation and causal relations via penalizing environmental heterogeneity. Our solution pertains to the second category, where the data distribution shifts across environments can be tethered by an invariant generation procedure [48, 53]. This work exploits the recovered causally invariant source representation to improve learning efficiency and mitigate the sample scarcity of minority labels in imbalanced sets.

Learning with imbalanced data. Resolving data imbalance is a heavily investigated topic [61]. Standard sampling and weight adjustments suffer from caveats such as introducing bias and information loss. Due to these concerns, recent literature has actively explored adaptive strategies, such as redundancy-adjusted balancing weights [22], and the theoretically grounded class-size adapted margins [10]. Similar to *boosting* [34], adaptive weights are designed to prioritize the learning of less well-classified examples [60] while excluding apparent outliers [59]. Much related to our setting are the *meta-learning* scenarios [88, 33, 90], where the model tries to generalize & repurpose the

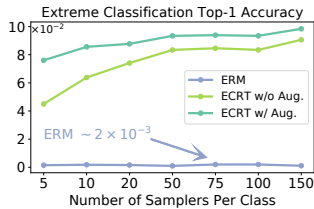


Figure 6: Extreme classification of $1k$ labels. ERM performs slightly better than random guess, while ECRT works significantly better.

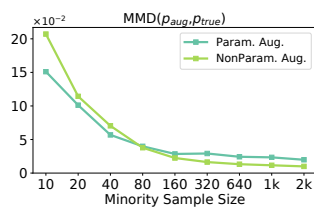


Figure 7: Comparison of different causal augmentations, lower is better. Parametric augmentation is more efficient with small samples.

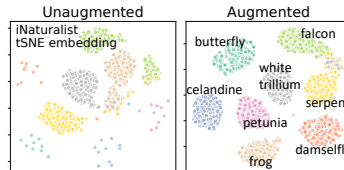


Figure 8: ECRT source representation trained on iNaturalist, visualized using tSNE embedding in two dimensions for eight random categories.

knowledge learned from majority classes to minority predictions; and also the augmentation-based schemes to restore class balance [64, 68].

Data augmentation. Due to its exceptional effectiveness, augmentation schemes are widely adopted in practical applications [77]. These augmentation strategies are built on known invariant transformations, *e.g.*, rotation, scaling, noise corruption, *etc.* [79], simple interpolation heuristics [11, 41], and more recently towards fully auto-mated procedures [21]. Notably, recent trend in data augmentation highlights robust learning against adversarially crafted inputs [35] and generative augmentation procedures that compose realistic artificial samples [3].

Domain adaption and causal mechanism transfer. Closest to our contribution is *causal mechanism transfer* (CMT) [83], which focused on addressing few-shot learning for continuous regression. We note a few key differences to our work: *(i)* CMT focused on domain adaptation and does not address classification; and *(ii)* it bundles (x, y) for NICA which necessitates the flow inversion for sample augmentation. Grounded in the setting of imbalanced data learning, our ECRT extends applications and advocates source space modeling to simplify and improve causal augmentation. It also features likelihood regularization to enhance representation regularity. We also offer new insights to justify the use of NICA-based augmentation, complementing the analysis from CMT by [83].

Energy-based modeling for representation learning. There is growing recognition that the energy perspective is integral to representation learning [58, 71, 82, 37]. In the lens of energy based modeling, the distribution of data is characterized as an (unnormalized) energy function [4]. Optimization of the energy function is often considered challenging [81] and contrastive techniques have been proven effective [44, 39]. Our work is a generalization of [48] that disentangles representations from an energy perspective. Interesting comparison can be made to [54], whose training objective bears resemblance to our ECRT. But the specific designs used by ECRT in the network architecture and scoring function allows ECRT to provably disentangle the feature representations and consequently capture causality for exploitation.

5 Experiments

To validate the utility of our model, we consider a wide range of (semi)-synthetic and real-world tasks experimentally. All experiments are implemented with PyTorch, and our code is available from <https://github.com/ZidiXiu/ECRT>. More details of our setup & additional analyses are deferred to the SM Sections C-E.

5.1 Experimental setup

Baselines. The following competing baselines are considered to benchmark the proposed solution: *(i)* Empirical risk minimization (ERM), a naïve baseline with no adjustment; *(ii)* Importance-weighting (IW) [9], a class-weight balanced training loss; *(iii)* Generative adversarial augmentation (GAN) [3], synthetic augmentations from adversarially-trained sampler; *(iv)* Virtual adversarial training (VAT) [66], robustness regularization with virtual perturbations; *(v)* FOCAL loss [60], cost-sensitive adaptive weighting; *(vi)* Label-distribution-aware margin loss (LDAM) [10], margin-optimal class weights. All baselines are tuned for best performance for TOP-1 accuracy on validation.

Evaluation metrics & setup. We consider the following metrics to quantitatively assess performance: *(i)* negative log-likelihood (NLL); *(ii)* F1 score; *(iii)* TOP- k accuracy ($k = 1, 5$). Following the classical evaluation setup for imbalanced data learning, we learn on an imbalanced training set and report performance on a balanced validation set.

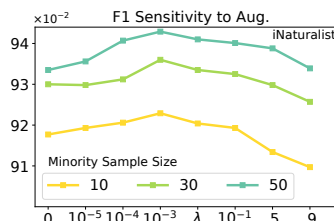
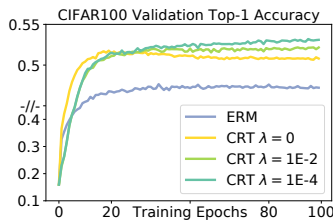
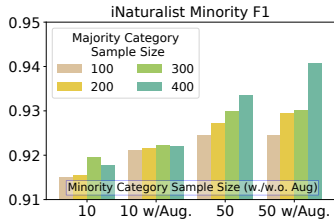


Figure 9: Performance comparison with and without augmentation. Augmented solutions improve the effective sample size.

Figure 10: Comparison of learning dynamics. ECRT enables both faster learning and better model predictions.

Figure 11: Sensitivity analysis of augmentation strength λ . Smaller minority sample sizes are more sensitive to the augmentation.

Table 1: Comparison of performance on real-world datasets (\uparrow higher is better, \downarrow lower is better).

	CIFAR100			iNATURALIST			TINYIMAGENET			ARXIV	
	TOP-1 \uparrow	TOP-5 \uparrow	NLL \downarrow	TOP-1 \uparrow	TOP-5 \uparrow	NLL \downarrow	TOP-1 \uparrow	TOP-5 \uparrow	NLL \downarrow	ACC \uparrow	NLL \downarrow
ERM	49.29	78.22	2.95	66.73	87.86	1.70	58.52	79.01	3.22	44.64	0.0407
IW	43.97	68.96	3.89	67.63	88.94	1.66	60.50	80.23	2.92	46.02	0.0477
GAN	47.64	78.53	2.69	67.40	87.00	1.82	60.69	80.91	2.33	45.42	0.0407
VAT	46.47	74.23	3.19	67.06	87.39	1.90	59.69	82.05	2.42	45.82	0.0474
FOCAL	43.32	74.39	2.89	66.63	88.45	1.59	58.27	79.39	2.59	46.01	0.0416
LDAM	50.46	74.39	2.18	67.39	87.13	4.00	58.18	82.51	2.15	45.04	0.0450
ECRT-1P	52.31	81.14	1.98	68.38	88.13	1.48	62.46	83.50	1.79	48.33	0.0434
ECRT-MP	53.00	81.99	2.31	69.01	90.01	1.23	64.40	84.54	1.94		

Toy model. We sample 2D standard Gaussians with different means and variances as source representation \mathbf{s} for each label class, which is then distorted by random affine and Hénon transformations $z_1 = 1 - 1.4\tilde{s}_1^2 + \tilde{s}_2$, $z_2 = 0.3\tilde{s}_1$, to induce real-world-like complex association structures. See the SM Sec. D for a detailed description and visualizations.

Real-world datasets. We consider the following semi-synthetic and real datasets: (i) Imbalanced MNIST and CIFAR100: standard image classification tasks with artificially created step-imbalanced following [10]; (ii) Imbalanced TinyImageNet [2]: a scaled-down version of the classic natural image dataset ImageNet, comprised of 200 classes, 500 samples per class and 10k validation images, with different simulated imbalances applied; (iii) iNaturalist 2019 [86]: a challenging task for image classification in the wild comprised of 26k training and 3k validation images labeled with 1k classes, with a skewed distribution in label frequency; (iv) arXiv abstracts, imbalanced multi-label prediction of paper categories with 160k samples and 152 classes.

Preprocessing, model architecture, and tuning. We use pre-trained models to extract vectorized representations for big complex datasets: ResNet [42] for image models of TinyImageNet², Inception V3 for iNaturalist³, and BERT [26]⁴ for the arXiv [1] language model. These pre-trained representations are used as raw feature inputs, subsequently fed into a fully-connected multi-layer perceptrons (MLP) for source space encoding. For small image models (*i.e.*, MNIST, CIFAR100) we directly train a CNN from scratch for feature extraction. We used a random 8/2 split for training and validation, and applied Adam optimizers for training. We rely on the best out-of-sample cross-entropy and GCL loss for hyperparameter tuning.

ECRT efficiency. We first examine the dynamics of efficiency gains from ECRT using a toy model, with the results summarized in Figure 9. Consistent with the shared embedding perspective, increasing the majority sample size improves the minority accuracy. Causal augmentation consistently improves performance, and it is most effective in the low-sample regime, offering more than 4 \times boosts in effective minority sample size. In Figure 10, we compare modeling with feature and source representations, respectively. Source space modeling speeds up learning, in addition to the modest accuracy gains. Augmented training is slightly slower, but eventually converges to a better solution.

²<https://download.pytorch.org/models/resnet18-5c106cde.pth>

³https://download.pytorch.org/models/inception_v3_google-1a9a5a14.pth

⁴<https://github.com/allenai/scibert>

Interestingly, the major performance gain originates from the GCL-based source space modeling we proposed, and to a lesser extent, from the augmentation perspective presented by [83].

Ablations on augmentation. We examined the contributions from augmentation as we vary the augmentation strength λ (Figure 11). A relatively small λ already yields improvement, but when the minority size is small, stronger augmentation degrades performance. This implies the augmentation gains are more likely to be originated from the exposure to the diversity of synthetic augmenting, and the accuracy of augmented distribution is limited by the imperfectness of empirical estimation (*e.g.*, limited sample size). In Figure 7 we compare the MMD distance [36] between the parametric and nonparametric augmentation outputs and the ground-truth, confirming the improved efficiency from the ECRT parametric augmentation in the low-sample regime.

Ablation on different model variants. We further compare the model performance with feature encoder trained with both majority and minority. (Table 1 used feature encoder trained only majority classes.) We have `Cifar100` TOP-1=51.79, TOP-5=81.02, NLL=2.03. This is slightly worse than the majority-only result but still outperformed other competing solutions. We caution, whether including minority examples in the pre-training of feature encoder differs case-by-case. They may not affect performance at all (majority dominant), improve performance (predictive features consistent with those used by majority) and completely devastating (containing spurious features, overfit).

Extreme classification. A related challenge of interest is extreme classification [16], where the label size is huge but there is only a handful of samples pertaining to each label class, This means there is no clear majority class. In Figure 6, we show the proposed ECRT also fares very well in this scenario, while standard ERM struggles (slightly better than random guess). This result evidences that ECRT also efficiently extracts generalizable information from an abundance of different class labels.

Imbalanced data learning. In Table 1 we compare the performance of ECRT to other competing solutions, with each baseline carefully tuned to ensure fairness. Minor discrepancies compared to results reported by prior literature are explained in the SM Sec. E, and in general our implementation performs slightly better. Overall, ECRT-based solutions consistently lead the performance chart, with the label-prior variant solidly outperforming vanilla ECRT and other competitors in most categories. While showing varying degrees of success, FOCAL and LDAM failed to establish dominance compared to ERM. GAN and VAT also verified the effectiveness of augmentation and adversarial perturbations in the imbalanced setting. We also compare the overall F1-score between different methods on `CIFAR100` dataset: ERM: 0.439, SMOTE [11]: 0.444, FOCAL:0.391, LDAM: 0.408, and ECRT: 0.482. FOCAL and LDAM gave very poor F1 scores in this case, even worse than the ERM baseline. SMOTE improved ERM, but the largest gain is obtained by ECRT. Figure 1 compares performance of different learning schemes condition on different label sizes using the F1 score on the `iNaturalist` data. In Figure 8 we show the ECRT learned representations, with and without augmentation, using tSNE embeddings.

6 Conclusion

This paper developed a novel learning scheme for imbalanced data learning. Leveraging a causal perspective, our solution cuts through the apparent data heterogeneity and identifies a shared, invariant, disentangled source representation, using only majority samples. We demonstrate this source representation modeling enables more efficient learning and allows principled augmentation. Importantly, we bridge the research between contrastive representation learning and energy modeling to causal machine learning, which constructs promising directions for future research.

Acknowledgements

This research was supported in part by NIH/NIDDK R01-DK123062, NIH/NIBIB R01-EB025020, NIH/NINDS 1R61NS120246, DARPA, DOE, ONR and NSF. J. Chen was partially supported by Shanghai Municipal Science and Technology Major Project (No.2018SHZDZX01) and National Key R&D Program of China (No.2018AAA0100303). This work used the Extreme Science and Engineering Discovery Environment (XSEDE), which is supported by National Science Foundation grant number ACI-1548562 [85]. This work used the Extreme Science and Engineering Discovery Environment (XSEDE) PSC Bridges-2 and SDSC Expanse at the service-provider through allocation TG-ELE200002 and TG-CIS210044.

References

- [1] Arxiv dataset. <https://www.kaggle.com/Cornell-University/arxiv>.
- [2] Tiny IMAGENET visual recognition challenge. <https://www.kaggle.com/c/tiny-imagenet>.
- [3] Antreas Antoniou, Amos Storkey, and Harrison Edwards. Data augmentation generative adversarial networks. *arXiv preprint arXiv:1711.04340*, 2017.
- [4] Michael Arbel, Liang Zhou, and Arthur Gretton. Generalized energy based models. In *ICLR*, 2020.
- [5] Martin Arjovsky, Léon Bottou, Ishaan Gulrajani, and David Lopez-Paz. Invariant risk minimization. *arXiv preprint arXiv:1907.02893*, 2019.
- [6] Nitin Bansal, Xiaohan Chen, and Zhangyang Wang. Can we gain more from orthogonality regularizations in training deep networks? In *NeurIPS*, 2018.
- [7] Zdravko I Botev and Dirk P Kroese. An efficient algorithm for rare-event probability estimation, combinatorial optimization, and counting. *Methodology and Computing in Applied Probability*, 10(4):471–505, 2008.
- [8] Peter Bühlmann. Invariance, causality and robustness. *arXiv preprint arXiv:1812.08233*, 2018.
- [9] Jonathon Byrd and Zachary Lipton. What is the effect of importance weighting in deep learning? In *ICML*, 2019.
- [10] Kaidi Cao, Colin Wei, Adrien Gaidon, Nikos Arechiga, and Tengyu Ma. Learning imbalanced datasets with label-distribution-aware margin loss. In *NeurIPS*, 2019.
- [11] Nitesh V Chawla, Kevin W Bowyer, Lawrence O Hall, and W Philip Kegelmeyer. SMOTE: synthetic minority over-sampling technique. *Journal of artificial intelligence research*, 16:321–357, 2002.
- [12] Junya Chen, Jianfeng Feng, and Wenlian Lu. A wiener causality defined by divergence. *Neural Processing Letters*, 53(3):1773–1794, 2021.
- [13] Junya Chen, Zhe Gan, Xuan Li, Qing Guo, Liqun Chen, Shuyang Gao, Tagyoung Chung, Yi Xu, Belinda Zeng, Wenlian Lu, et al. Simpler, faster, stronger: Breaking the log-k curse on contrastive learners with flatnce. *arXiv preprint arXiv:2107.01152*, 2021.
- [14] Junya Chen, Danni Lu, Zidi Xiu, Ke Bai, Lawrence Carin, and Chenyang Tao. Variational inference with holder bounds. *arXiv preprint arXiv:2111.02947*, 2021.
- [15] Ting Chen, Simon Kornblith, Mohammad Norouzi, and Geoffrey Hinton. A simple framework for contrastive learning of visual representations. In *ICML*, 2020.
- [16] Anna Choromanska, Alekh Agarwal, and John Langford. Extreme multi class classification. In *NIPS Workshop: eXtreme Classification, submitted*, 2013.
- [17] Alexandra Chouldechova and Aaron Roth. The frontiers of fairness in machine learning. *arXiv preprint arXiv:1810.08810*, 2018.
- [18] Michael Cogswell, Faruk Ahmed, Ross Girshick, Larry Zitnick, and Dhruv Batra. Reducing overfitting in deep networks by decorrelating representations. *arXiv preprint arXiv:1511.06068*, 2015.
- [19] Pierre Comon. Independent component analysis, a new concept? *Signal processing*, 36(3):287–314, 1994.
- [20] Corinna Cortes and Vladimir Vapnik. Support-vector networks. *Machine learning*, 20(3):273–297, 1995.
- [21] Ekin D Cubuk, Barret Zoph, Dandelion Mane, Vijay Vasudevan, and Quoc V Le. Autoaugment: Learning augmentation strategies from data. In *CVPR*, 2019.
- [22] Yin Cui, Menglin Jia, Tsung-Yi Lin, Yang Song, and Serge Belongie. Class-balanced loss based on effective number of samples. In *CVPR*, 2019.
- [23] Bo Dai, Zhen Liu, Hanjun Dai, Niao He, Arthur Gretton, Le Song, and Dale Schuurmans. Exponential family estimation via adversarial dynamics embedding. In *NeurIPS*, pages 10979–10990, 2019.
- [24] Andrea Dal Pozzolo, Giacomo Boracchi, Olivier Caelen, Cesare Alippi, and Gianluca Bontempi. Credit card fraud detection: a realistic modeling and a novel learning strategy. *IEEE transactions on neural networks and learning systems*, 29(8):3784–3797, 2017.

- [25] Guillaume Desjardins, Karen Simonyan, Razvan Pascanu, et al. Natural neural networks. In *NIPS*, 2015.
- [26] Jacob Devlin, Ming-Wei Chang, Kenton Lee, and Kristina Toutanova. Bert: Pre-training of deep bidirectional transformers for language understanding. In *NAACL*, 2019.
- [27] Thomas A Dingus, Feng Guo, Suzie Lee, Jonathan F Antin, Miguel Perez, Mindy Buchanan-King, and Jonathan Hankey. Driver crash risk factors and prevalence evaluation using naturalistic driving data. *Proceedings of the National Academy of Sciences*, 113(10):2636–2641, 2016.
- [28] Monroe D Donsker and SR Srinivasa Varadhan. Asymptotic evaluation of certain markov process expectations for large time. iv. *Communications on Pure and Applied Mathematics*, 36(2):183–212, 1983.
- [29] Chris Drummond, Robert C Holte, et al. C4. 5, class imbalance, and cost sensitivity: why under-sampling beats over-sampling. In *Workshop on learning from imbalanced datasets II*, volume 11, pages 1–8. Citeseer, 2003.
- [30] Charles Elkan. The foundations of cost-sensitive learning. In *International joint conference on artificial intelligence*, volume 17, pages 973–978. Lawrence Erlbaum Associates Ltd, 2001.
- [31] Li Fei-Fei, Rob Fergus, and Pietro Perona. One-shot learning of object categories. *IEEE transactions on pattern analysis and machine intelligence*, 28(4):594–611, 2006.
- [32] Werner Fenchel. On conjugate convex functions. *Canadian Journal of Mathematics*, 1(1):73–77, 1949.
- [33] Chelsea Finn, Pieter Abbeel, and Sergey Levine. Model-agnostic meta-learning for fast adaptation of deep networks. *arXiv preprint arXiv:1703.03400*, 2017.
- [34] Yoav Freund and Robert E Schapire. A decision-theoretic generalization of on-line learning and an application to boosting. *Journal of computer and system sciences*, 55(1):119–139, 1997.
- [35] Ian J Goodfellow, Jonathon Shlens, and Christian Szegedy. Explaining and harnessing adversarial examples. In *ICLR*, 2015.
- [36] Arthur Gretton, Karsten M Borgwardt, Malte J Rasch, Bernhard Schölkopf, and Alexander Smola. A kernel two-sample test. *Journal of Machine Learning Research*, 13(Mar):723–773, 2012.
- [37] Qing Guo, Junya Chen, Dong Wang, Yuewei Yang, Xinwei Deng, Fan Li, Lawrence Carin, and Chenyang Tao. Tight mutual information estimation with contrastive Fenchel-Legendre optimization, 2021. [Available online; accessed 28-May-2021].
- [38] Michael Gutmann and Jun-ichiro Hirayama. Bregman divergence as general framework to estimate unnormalized statistical models. *arXiv preprint arXiv:1202.3727*, 2012.
- [39] Michael Gutmann and Aapo Hyvärinen. Noise-contrastive estimation: A new estimation principle for unnormalized statistical models. In *AISTATS*, pages 297–304. JMLR Workshop and Conference Proceedings, 2010.
- [40] Bharath Hariharan and Ross Girshick. Low-shot visual recognition by shrinking and hallucinating features. In *ICCV*, pages 3018–3027, 2017.
- [41] Haibo He, Yang Bai, Eduardo A Garcia, and Shutao Li. Adasyn: Adaptive synthetic sampling approach for imbalanced learning. In *WCCI*, 2008.
- [42] Kaiming He, Xiangyu Zhang, Shaoqing Ren, and Jian Sun. Deep residual learning for image recognition. In *CVPR*, 2016.
- [43] Christina Heinze-Deml, Jonas Peters, and Nicolai Meinshausen. Invariant causal prediction for nonlinear models. *Journal of Causal Inference*, 6(2), 2018.
- [44] Geoffrey E Hinton. Training products of experts by minimizing contrastive divergence. *Neural computation*, 14(8):1771–1800, 2002.
- [45] Lei Huang, Dawei Yang, Bo Lang, and Jia Deng. Decorrelated batch normalization. In *CVPR*, 2018.
- [46] Aapo Hyvärinen and Erkki Oja. Independent component analysis: algorithms and applications. *Neural networks*, 13(4-5):411–430, 2000.
- [47] Aapo Hyvärinen and Petteri Pajunen. Nonlinear independent component analysis: Existence and uniqueness results. *Neural networks*, 12(3):429–439, 1999.

- [48] Aapo Hyvarinen, Hiroaki Sasaki, and Richard Turner. Nonlinear ica using auxiliary variables and generalized contrastive learning. In *AISTATS*, pages 859–868, 2019.
- [49] Kui Jia, Shuai Li, Yuxin Wen, Tongliang Liu, and Dacheng Tao. Orthogonal deep neural networks. *IEEE transactions on pattern analysis and machine intelligence*, 2019.
- [50] I Kaggle. Planet: Understanding the amazon from space kaggle. Consulté sur <https://www.kaggle.com/c/planet-understanding-the-amazon-from-space/data> (Consulté le: 2018-01-25), 2017.
- [51] Bingyi Kang, Saining Xie, Marcus Rohrbach, Zhicheng Yan, Albert Gordo, Jiashi Feng, and Yannis Kalantidis. Decoupling representation and classifier for long-tailed recognition. In *ICLR*, 2019.
- [52] Agnan Kessy, Alex Lewin, and Korbinian Strimmer. Optimal whitening and decorrelation. *The American Statistician*, 72(4):309–314, 2018.
- [53] Ilyes Khemakhem, Diederik Kingma, Ricardo Monti, and Aapo Hyvarinen. Variational autoencoders and nonlinear ICA: A unifying framework. In *AISTATS*, pages 2207–2217, 2020.
- [54] Prannay Khosla, Piotr Teterwak, Chen Wang, Aaron Sarna, Yonglong Tian, Phillip Isola, Aaron Maschiot, Ce Liu, and Dilip Krishnan. Supervised contrastive learning. In *NeurIPS*, volume 33, 2020.
- [55] Jaehyung Kim, Jongheon Jeong, and Jinwoo Shin. M2m: Imbalanced classification via major-to-minor translation. In *CVPR*, pages 13896–13905, 2020.
- [56] Gary King and Langche Zeng. Logistic regression in rare events data. *Political analysis*, 9(2):137–163, 2001.
- [57] Sotiris Kotsiantis, Dimitris Kanellopoulos, Panayiotis Pintelas, et al. Handling imbalanced datasets: A review. *GESTS International Transactions on Computer Science and Engineering*, 30(1):25–36, 2006.
- [58] Yann LeCun, Sumit Chopra, Raia Hadsell, Marc’Aurelio Ranzato, and Fu-Jie Huang. *Predicting Structured Data*, chapter A Tutorial on Energy-Based Learning. MIT Press, 2006.
- [59] Buyu Li, Yu Liu, and Xiaogang Wang. Gradient harmonized single-stage detector. In *AAAI*, 2019.
- [60] Tsung-Yi Lin, Priya Goyal, Ross Girshick, Kaiming He, and Piotr Dollár. Focal loss for dense object detection. In *ICCV*, 2017.
- [61] Ziwei Liu, Zhongqi Miao, Xiaohang Zhan, Jiayun Wang, Boqing Gong, and Stella X Yu. Large-scale long-tailed recognition in an open world. In *CVPR*, 2019.
- [62] Danni Lu, Chenyang Tao, Junya Chen, Fan Li, Feng Guo, and Lawrence Carin. Reconsidering generative objectives for counterfactual reasoning. In *NeurIPS*, 2020.
- [63] JA Tenreiro Machado and António M Lopes. Rare and extreme events: the case of covid-19 pandemic. *Nonlinear Dynamics*, page 1, 2020.
- [64] Giovanni Mariani, Florian Scheidegger, Roxana Istrate, Costas Bekas, and Cristiano Malossi. BAPAN: Data augmentation with balancing GAN. *arXiv preprint arXiv:1803.09655*, 2018.
- [65] Aditya Krishna Menon, Sadeep Jayasumana, Ankit Singh Rawat, Himanshu Jain, Andreas Veit, and Sanjiv Kumar. Long-tail learning via logit adjustment. In *ICLR*, 2020.
- [66] Takeru Miyato, Shin-ichi Maeda, Masanori Koyama, and Shin Ishii. Virtual adversarial training: a regularization method for supervised and semi-supervised learning. *IEEE transactions on pattern analysis and machine intelligence*, 41(8):1979–1993, 2018.
- [67] Mary M Moya and Don R Hush. Network constraints and multi-objective optimization for one-class classification. *Neural networks*, 9(3):463–474, 1996.
- [68] Sankha Subhra Mullick, Shounak Datta, and Swagatam Das. Generative adversarial minority oversampling. In *ICCV*, 2019.
- [69] George Papamakarios, Theo Pavlakou, and Iain Murray. Masked autoregressive flow for density estimation. In *NIPS*, 2017.
- [70] Jonas Peters, Peter Bühlmann, and Nicolai Meinshausen. Causal inference using invariant prediction: identification and confidence intervals. *Journal of the Royal Statistical Society Series B (Statistical Methodology)*, 2016.

- [71] Ben Poole, Sherjil Ozair, Aaron Van Den Oord, Alex Alemi, and George Tucker. On variational bounds of mutual information. In *ICML*. PMLR, 2019.
- [72] Joshua Robinson, Stefanie Jegelka, and Suvrit Sra. Strength from weakness: Fast learning using weak supervision. In *ICML*, 2020.
- [73] Mateo Rojas-Carulla, Bernhard Schölkopf, Richard Turner, and Jonas Peters. Invariant models for causal transfer learning. *The Journal of Machine Learning Research*, 19(1):1309–1342, 2018.
- [74] Dominik Rothenhäusler, Nicolai Meinshausen, Peter Bühlmann, and Jonas Peters. Anchor regression: heterogeneous data meets causality. *arXiv preprint arXiv:1801.06229*, 2018.
- [75] Lukas Ruff, Robert Vandermeulen, Nico Goernitz, Lucas Deecke, Shoaib Ahmed Siddiqui, Alexander Binder, Emmanuel Müller, and Marius Kloft. Deep one-class classification. In *ICML*, 2018.
- [76] Bernhard Schölkopf, Dominik Janzing, Jonas Peters, Eleni Sgouritsa, Kun Zhang, and Joris Mooij. On causal and anticausal learning. *arXiv preprint arXiv:1206.6471*, 2012.
- [77] Connor Shorten and Taghi M Khoshgoftaar. A survey on image data augmentation for deep learning. *Journal of Big Data*, 6(1):60, 2019.
- [78] Narayanaswamy Siddharth, Brooks Paige, Jan-Willem Van de Meent, Alban Desmaison, Noah Goodman, Pushmeet Kohli, Frank Wood, and Philip Torr. Learning disentangled representations with semi-supervised deep generative models. In *NIPS*, 2017.
- [79] Christian Szegedy, Vincent Vanhoucke, Sergey Ioffe, Jon Shlens, and Zbigniew Wojna. Rethinking the inception architecture for computer vision. In *CVPR*, 2016.
- [80] Kaihua Tang, Jianqiang Huang, and Hanwang Zhang. Long-tailed classification by keeping the good and removing the bad momentum causal effect. In *NeurIPS*, volume 33, 2020.
- [81] Chenyang Tao, Liqun Chen, Shuyang Dai, Junya Chen, Ke Bai, Dong Wang, Jianfeng Feng, Wenlian Lu, Georgiy V Bobashev, and Lawrence Carin. On fenchel mini-max learning. In *NeurIPS*, 2019.
- [82] Chenyang Tao, Shuyang Dai, Liqun Chen, Ke Bai, Junya Chen, Chang Liu, Ruiyi Zhang, Georgiy Bobashev, and Lawrence Carin Duke. Variational annealing of gans: A langevin perspective. In *ICML*, pages 6176–6185. PMLR, 2019.
- [83] Takeshi Teshima, Issei Sato, and Masashi Sugiyama. Few-shot domain adaptation by causal mechanism transfer. In *ICML*, 2020.
- [84] Pavel Tokmakov, Yu-Xiong Wang, and Martial Hebert. Learning compositional representations for few-shot recognition. In *ICCV*, 2019.
- [85] John Towns, Timothy Cockerill, Maytal Dahan, Ian Foster, Kelly Gauthier, Andrew Grimshaw, Victor Hazlewood, Scott Lathrop, Dave Lifka, Gregory D Peterson, et al. Xsede: accelerating scientific discovery. *Computing in science & engineering*, 16(5):62–74, 2014.
- [86] Grant Van Horn, Oisín Mac Aodha, Yang Song, Yin Cui, Chen Sun, Alex Shepard, Hartwig Adam, Pietro Perona, and Serge Belongie. The iNaturalist species classification and detection dataset. In *CVPR*, 2018.
- [87] Vladimir Vapnik. *The nature of statistical learning theory*. Springer science & business media, 2013.
- [88] Oriol Vinyals, Charles Blundell, Timothy Lillicrap, Daan Wierstra, et al. Matching networks for one shot learning. In *NIPS*, 2016.
- [89] Yaqing Wang, Quanming Yao, James T Kwok, and Lionel M Ni. Generalizing from a few examples: A survey on few-shot learning. *ACM Computing Surveys*, 53(3):1–34, 2020.
- [90] Yu-Xiong Wang, Deva Ramanan, and Martial Hebert. Learning to model the tail. In *NIPS*, 2017.
- [91] Zidi Xiu, Chenyang Tao, Michael Gao, Connor Davis, Benjamin Goldstein, and Ricardo Henao. Variational disentanglement for rare event modeling. In *AAAI*, 2021.
- [92] Zidi Xiu, Chenyang Tao, and Ricardo Henao. Variational learning of individual survival distributions. In *ACM CHIL*, 2020.

Supercharging Imbalanced Data Learning With Energy-based Contrastive Representation Transfer (Supplementary Material)

Zidi Xiu, Junya Chen, Benjamin Goldstein, Ricardo Henao, Lawrence Carin, Chenyang Tao
Duke University

Contents

A Theoretical Support	1
A.1 Nonlinear ICA with auxiliary variables	1
A.2 Variance and generalization bound	2
A.3 Speedup from shared embedding	3
A.4 Energy-based GCL	3
A.5 Invertible neural network	4
B Regression for continuous labels	4
C Implementation of Augmentation	4
D Toy Model Experiment	5
D.1 Toy data demo	5
D.2 Extreme-classification Toy Data	5
E Real-world Data Experiments	6
E.1 Image Data Benchmarks	6
E.2 Language Data Benchmark	6

A. Theoretical Support

Here we summarize some theories from literature that supports the development of this paper by making it self-contained. Attempts have been made to unify the notations, making them consistent with our paper, and also drop some contents from the original presentations that not directly relevant in this context.

A.1. Nonlinear ICA with auxiliary variables

The following theory lists the technical conditions required for the identification of conditional nonlinear ICA model, based on which our work was built.

Definition A.1 (Conditionally exponential of order k). A random variable (independent component) $[s]_i$ is conditionally exponential of order k given random vector \mathbf{c} if its conditional pdf can be given in the form

$$p([s]_i|\mathbf{c}) = \frac{Q_i([s]_i)}{Z_i(\mathbf{c})} \exp \left[\sum_{j=1}^k \tilde{q}_{ij}([s]_i) \lambda_{ij}(\mathbf{c}) \right] \quad (\text{S1})$$

almost everywhere in the support of \mathbf{c} , with $\tilde{q}_{ij}, \lambda_{ij}, Q_i$ and Z_i scalar-valued functions. The sufficient statistics \tilde{q}_{ij} are assumed linearly independent.

Theorem A.2 (Theorem 3, [4], identification of Nonlinear ICA). *Assume (i) the data follows the nonlinear ICA model with the conditional independence $q(\mathbf{s}|\mathbf{c}) = \prod_j q_j([\mathbf{s}]_j|\mathbf{c})$; (ii) Each $[\mathbf{s}]_j$ is conditionally exponential given \mathbf{c} (Definition A.1); (iii) There exist $nk + 1$ points $\mathbf{c}_0, \dots, \mathbf{c}_{nk}$, such that the following matrix of size $nk \times nk$*

$$\tilde{\mathbf{L}} = \begin{pmatrix} \lambda_{11}(\mathbf{c}_1) - \lambda_{11}(\mathbf{c}_0) & \cdots & \lambda_{11}(\mathbf{c}_{nk}) - \lambda_{11}(\mathbf{c}_0) \\ \lambda_{nk}(\mathbf{c}_1) - \lambda_{nk}(\mathbf{c}_0) & \cdots & \lambda_{nk}(\mathbf{c}_{nk}) - \lambda_{nk}(\mathbf{c}_0) \end{pmatrix} \quad (\text{S2})$$

is invertible; (iv) nonlinear Logistic regression system Eqn (1) is trained using functions with universal approximation capacity. Then in the limit of infinite data, $f(\mathbf{z})$ provides a consistent estimator of the nonlinear ICA model, up to a linear transformation of point-wise scalar functions of the independent components.

A.2. Variance and generalization bound

The following theories explore the consequence of training using only nonparametric causal augmentation. First we define the risk estimators.

Definition A.3. Let \tilde{S} be the non-parametric source augmentation defined in Eqn (3) main text, $\ell(\cdot)$ be the loss function, $g(\mathbf{z})$ be the hypothesis function. We define the risk R and causally augmented risk estimator \check{R} wrt g respectively as

$$R(g) \triangleq \mathbb{E}_Z[\ell(g(Z))], \check{R}(g) \triangleq \mathbb{E}_{\tilde{S}}[\ell(g(\hat{f}^{-1}(\tilde{S})))], \quad (\text{S3})$$

where \hat{f} is the estimated causal de-mixing function.

The following theorem revealed that assuming perfect knowledge of de-mixing function f , the causally augmented risk estimator is optimal.

Proposition A.4. Assuming $\hat{f} = f$, and let $\ell(h(\mathbf{x}), y)$ be the classification loss for predictor $h \in \mathcal{H}$. Let $\hat{R}(h) = \sum_m w_m \hat{R}_m(h)$ be an estimator for $R(h) = \mathbb{E}[\ell(h(\mathbf{x}), y)]$, such that $\hat{R}(h)$ is an unbiased estimator for $R_m(h) = \mathbb{E}_{y=m}[\ell(h(\mathbf{x}), y)]$. Then $\tilde{R}(h) = \sum_m w_m \tilde{R}_m(h)$, where $\tilde{R}_m(h) \triangleq \mathbb{E}_{y_i=m}[\ell(h(\tilde{\mathbf{x}}_i), y_i)]$ is the minimum variance unbiased estimator among all $\hat{R}(h)$.

Proof. This is a direct consequence of Theorem A.5. If $\tilde{R}(h)$ is not the minimal variance estimator, then at least one of $\tilde{R}_m(h)$ is not optimal, which contradicts Theorem A.5. \square

Theorem A.5 (Theorem 1, [9], minimum variance property). *Assuming $\hat{f} = f$. Then for each $g \in \mathcal{G}$, the causal augmented risk estimator $\check{R}(g)$ is the uniformly minimum variance unbiased estimator of $R(g)$, i.e., $\mathbb{E}[\check{R}(g)] = R(g)$ and for any unbiased estimator \check{R} of $R(g)$ (i.e., $\mathbb{E}[\check{R}(g)] = R(g)$),*

$$\text{Var}[\check{R}(g)] \leq \text{Var}[\check{R}(g)]. \quad (\text{S4})$$

Since we are bound to have estimation errors, the next theorem establishes the generalization bounds wrt such errors.

Theorem A.6 (Theorem 2, [9], excess risk bound). *Let $\check{g} = \arg \min \check{R}$ and $g^* = \arg \min R(g)$, then under appropriate assumptions (Assumptions 1-8 in [9]), for arbitrary $\delta, \delta' \in (0, 1)$, we have probability at least $1 - (\delta + \delta')$,*

$$R(\check{g}) - R(g^*) \leq \underbrace{C \sum_{j=1}^d \|f_j - \hat{f}\|_{W^{1,1}}}_{\text{Approximation error}} + \underbrace{4d\mathfrak{R}(\mathcal{G}) + 2dB_\ell \sqrt{\frac{\log 2/\delta}{2n}}}_{\text{Estimation error}} + \underbrace{\kappa_1(\delta', n) + dB_\ell B_q \kappa_2(f - \hat{f})}_{\text{Higher-order terms}}. \quad (\text{S5})$$

Here $\|\cdot\|_{W^{1,1}}$ is the Sobolev norm and $\mathfrak{R}(\mathcal{G})$ is the effective Rademacher complexity defined by

$$\mathfrak{R}(\mathcal{G}) \triangleq \frac{1}{n} \mathbb{E}_{\tilde{S}} \mathbb{E}_{\sigma} \left[\sup_{g \in \mathcal{G}} \left| \sum_{i=1}^n \sigma_i s \mathbb{E}_{S_2, \dots, S_d} \tilde{\ell}(\hat{s}_i, S'_2, \dots, S'_d) \right| \right], \quad (\text{S6})$$

where $\{\sigma_i\}_{i=1}^n$ are independent sign variables, $\mathbb{E}_{\hat{s}}$ is the expectation wrt $\{\hat{s}_i\}_{i=1}^n$, the dummy variables S'_2, \dots, S'_d are i.i.d. copies of \hat{s}_1 , and $\tilde{\ell}$ is defined by

$$\tilde{\ell}(s_1, \dots, s_d) \triangleq \frac{1}{d!} \sum_{\pi} \ell(g, \hat{f}^{-1}(s_{\pi(1)}, \dots, s_{\pi(d)})), \quad (\text{S7})$$

where π denotes the permutations. κ_1, κ_2 are higher order terms, B_q, B_ℓ respectively depends on density q and loss ℓ , while C' depends on (f, q, ℓ, d) .

A.3. Speedup from shared embedding

[8] built some interesting theories trying to answer the following question: “Can large amounts of weakly labeled data provably help learn a better model than strong labels alone?” The answer is positive, assuming there is a shared embedding between the *weak* and *strong* tasks, which respectively refers auxiliary (secondary) and main tasks of interests. We summarize its main findings below and elaborate how it lends support for ECRT.

In the setting of weakly supervised learning, we have the triplet $(\mathcal{X}, \mathcal{W}, \mathcal{Y})$, where \mathcal{X} and \mathcal{Y} respectively denote the features and labels of interest (strong task), and \mathcal{W} denote weak task labels that are relevant to the prediction of \mathcal{Y} . It is assumed that there is this unknown good embedding $Z = f_0(X)$ that predicts W , that could be leveraged to derive a model of the form $\hat{g}(\cdot, \hat{f}) : \mathcal{X} \rightarrow \mathcal{Y}$ that improves learning.

Algorithm 1 Weakly supervised learning

1. Pretrain encoder with weak labels

$$\hat{f} \leftarrow \text{Alg}(\mathcal{F}, \mathbb{P}_{XW})$$

2. Augment data with

$$z_i = \hat{f}(x_i) \Rightarrow \{(x_i, y_i, z_i)\} \sim \hat{\mathbb{P}}_{XYZ}$$

3. Optimize the strong task

$$\hat{g} \leftarrow \text{Alg}(\mathcal{G}, \hat{\mathbb{P}}_{XYZ})$$

Theorem A.7 (Theorem 3, [8]). *Suppose that $\text{Rate}_m(\mathcal{F}, \mathbb{P}_{XW}) = \mathcal{O}(m^{-\alpha})$ and that $\text{Alg}_n(\mathcal{G}, \hat{\mathbb{P}})$ is ERM. Under suitable assumptions on $(\ell, \mathbb{P}, \mathcal{F})$, Algorithm 1 obtains excess risk*

$$\mathcal{O}\left(\frac{\alpha\beta \log n + \log(1/\delta)}{n} + \frac{1}{n^{\alpha\beta}}\right) \quad (\text{S8})$$

with probability $1 - \delta$, when $m = \Omega(n^\beta)$ for \mathcal{W} discrete, or $m = \Omega(n^{2\beta})$ for \mathcal{W} continuous.

For concrete examples, in a typical learning scenario where $\text{Alg}_m(\mathcal{F}, \mathbb{P}_{XW}) = \mathcal{O}(m^{-1/2})$, one obtains the fast rates $\mathcal{O}(1/n)$ for $m = \Omega(n^2)$.

In the context of our ECRT, we identify the learning of common causal de-mixing function $f(z)$ as the weak learning task, and the source space \mathcal{S} is the common embedding space of interest. This allows us to tap into the power of weakly supervised learning to improve the main classification task. See Figure 9 in the main text for evidence.

A.4. Energy-based GCL

Mutual information (MI) is a popular metric to quantify the associations between random variables, and has been applied to a lot of areas like independent component analysis, fair learning and etc. Inspired by the FDV loss introduced in [3], rooted from the MI between the feature z and label y . Following the Equation (4) in the main text for I_{FDV} , we have a novel MI objective, pointwise mutual information (PMI) which takes the place of logistic regression objective in GCL,

$$\mathcal{L}_{\text{FDV}}(f_\psi, g_\nu) \triangleq \hat{I}_{\text{DV}}(\{z_i, \mathbf{y}_i\}) + \frac{\sum_j \exp[(g_\nu(\mathbf{y}_j, z_i) - g_\nu(\mathbf{y}_i, z_i))/\tau]}{\sum_j \exp[(\hat{g}_\nu(\mathbf{y}_j, z_i) - \hat{g}_\nu(\mathbf{y}_i, z_i))/\tau]} - 1, \quad (\text{S9})$$

where \mathbf{y}_i is the embedding of label, τ is a learnable temperature parameter, $g_\nu(\mathbf{y}, z) = \text{sim}(\mathbf{y}, \sum_{a=1}^d \gamma_\nu^a(y, [\mathbf{s}]_a))$, and $\text{sim}(\mathbf{x}, \mathbf{y}) = \frac{\mathbf{x}^\top \mathbf{y}}{\|\mathbf{x}\| \|\mathbf{y}\|}$, γ_ν and \mathbf{s} are the same as Equation (1) with slightly change of dimension with linear transformations.

One notable difference between Equation (S9) and Equation (1) from the GCL lies in the negative sample size. In energy-based GCL, the model can treat all the examples within a minibatch as negative examples, while the original GCL contrasts with only one negative example in the minibatch by permutating labels. This refinement can benefit the learning efficiency of the NICA step, the correlation between labels decrease faster than the original GCL, as illustrated in Figure S1.

A.5. Invertible neural network

The recent interest in generative modeling has popularized the use of *invertible neural networks* (INN) in machine learning, with prominent examples such as normalizing flows [7] and neural ordinary differential equations (ODEs) [2]. Unlike standard neural networks, an INN seeks to establish a one-to-one mapping between the input and output domains, *i.e.*, the forward map $\mathbf{s} = f_\psi(\mathbf{z})$ as well as the corresponding inverse map $\mathbf{z} = f_\psi^{-1}(\mathbf{s})$. Standard constructions of INN achieve representational flexibility by stacking simple invertible transformations. In practice, the efficiency of the forward or inverse passes are often trade-off depending on the application needs [6]. Here we aim for fast forward computations, thus adopt the *masked auto-regressive flow* (MAF) design for our INN [6], which allows efficient parallelization of the autoregressive architecture via *causal masking*.

Let $\{\mathbf{z}^t\}_{t=0}^T$ be a flow of length T , in which $\mathbf{z}^0 = \mathbf{z}$, $\mathbf{z}^{t+1} = F_t(\mathbf{z}^t)$, $\mathbf{s} = \mathbf{z}^T$, and we let $f_\psi = F_1 \circ F_2 \cdots \circ F_{T-1}$. Specifically, the MAF is constructed as a series of *shift and scale* transformations $\mathbf{z}^{t+1} = F_t(\mathbf{z}^t) \triangleq \mathbf{a}_t(\mathbf{z}^t) \odot \mathbf{z}^t + \mathbf{b}_t(\mathbf{z}^t)$, where \odot is the element-wise product, and $\mathbf{a}_t(\cdot)$ and $\mathbf{b}_t(\cdot)$ are vector transformations known as scale and shift, respectively, that follow a causal autoregressive structure, *i.e.*, that $[\mathbf{z}^{t+1}]_k$ only depends on $[\mathbf{z}^t]_{<k}$. As a direct consequence of this structure, the MAF-based INN results in a tractable Jacobian $J(\mathbf{z}) \triangleq |\det(\nabla_{\mathbf{z}} f_\psi)|$ of $f_\psi(\mathbf{z})$ that facilitates likelihood computations. In fact, assuming the sources \mathcal{S} have prior density $p(\mathbf{s})$, the likelihood of the features $p(\mathbf{z})$ of the MAF specification is given by [6]:

$$\log p(\mathbf{z}) = \log |\det(\nabla_{\mathbf{z}} f_\psi)| + \log p(\mathbf{s}) = \sum_t \log |\mathbf{a}_t(\mathbf{z}^t)| + \log p(\mathbf{s}) \triangleq \mathcal{L}_{\text{FLOW}}(f_\psi) \tag{S10}$$

Jointly with $\mathcal{L}_{\text{GCL}}(f_\psi, r_\nu)$ (Equation (1) in the main text), $\mathcal{L}_{\text{FLOW}}(f_\psi)$ can be used to optimize the parameters of the de-mixing function $f_\psi(\mathbf{z})$.

B. Regression for continuous labels

We can further extend the applicability of the proposed ECRT to the case of regressing continuous outcomes. While in principle, the procedures described in Sec 3 can be readily applied, we advocate coarse graining wrt label y similar to what has been practiced in *sliced inverse regression* [5], especially when the feature dimension is high relative to the sample size. Specifically, we partition y into different bins, and use feed the bin label as the conditioning variable in the GCL step. We still use the regression loss for the training of encoder and predictors.

C. Implementation of Augmentation

Let $\hat{\mathbf{s}}_i^k, i = 1, \dots, n_k$ be the estimated source representation for the k -th class.

- Non-parametric augmentation: shuffling indices as described in the main text.
- Parametric augmentation: estimate $\hat{\mu}_k = \text{mean}(\hat{\mathbf{s}}^k), \hat{\sigma}_k = \text{std}(\hat{\mathbf{s}}^k)$, then $\mathbf{s}^{k, \text{aug}} \sim \mathcal{N}(\hat{\mu}_k, \hat{\sigma}_k^2)$.
- Oracle augmentation: nonparametric augmentation with an abundance of class-conditional source space samples .

In Figure 9 from main text we compare the efficiency of parametric and nonparametric augmentation schemes under different minority sample size. In particular, we compute the MMD distance $\|\hat{\mu}_{\text{aug}} - \hat{\mu}_{\text{ref}}\|_\kappa$, where $\hat{\mu}_{\text{aug}} = \sum_i \kappa(\tilde{s}_i, \cdot)$ and $\hat{\mu}_{\text{ref}} = \sum_i \kappa(s_i, \cdot)$. Here $\kappa(\cdot, \cdot)$ is the Gaussian rbf kernel $\kappa(x, y) = \exp(-\|x - y\|^2 / 2\sigma^2)$, $\|f\|_\kappa = \sqrt{\langle f, f \rangle_\kappa}$ is the RKHS norm and \tilde{s}_i, s_i respectively denote augmented class-conditional samples (from few minority samples) and empirical distribution of class-conditional samples (where we use all samples from the same class that we holdout). In this example we use $2k$

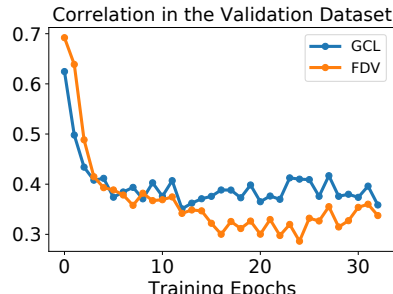


Figure S1. Comparison of correlation decreasing with GCL and FDV in the MNIST dataset. FDV approaches the optimality faster, which indicates better efficiency.

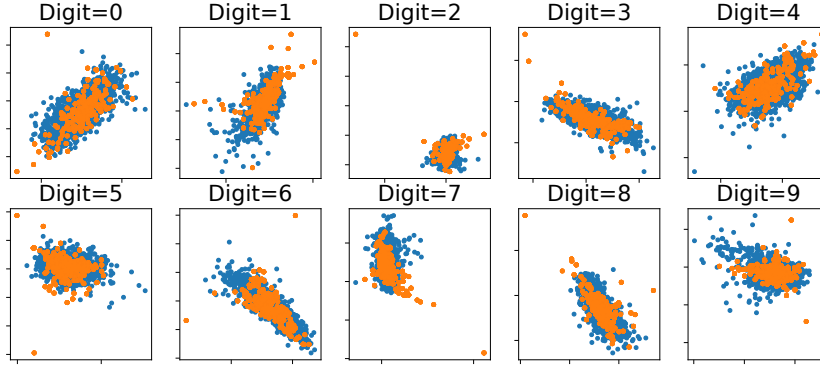


Figure S2. Feature space augmentation for MNIST.

samples for the ground truth and augment minority to the same size. Different kernel bandwidth σ of κ yields qualitatively similar results, and in the paper we report the one with $\sigma = 0.5$.

In Figure S2, we visualize the augmentation in feature space for the MNIST dataset. And we see for boundary points the discrepancy can be amplified by the neural network inversion, which partly explained the sub-optimal performance from feature space augmentation. In contrast, the source space augmentation advocated in this paper is more computationally efficient and robust.

Note that while in principle the majority classes can be similarly augmented, we choose not to refine our model with the augmented majorities. This decision is justified by the classical consideration for bias-variance trade-off: estimation errors of $f(z)$ is inevitable (*e.g.*, finite sample size, SGD, limited network capacity, *etc.*), and they will carry over to the augmented samples, resulting biases in the augmented estimation of our predictor. On the other hand, using augmented samples helps bring down estimation variance. For minority labels, the reduction in variance is greater than the induced bias, and consequently merits the application of ECRT to improve performance. For majority labels, this might not be the case.

D. Toy Model Experiment

D.1. Toy data demo

We sample seven groups of two-dimensional uncorrelated Gaussian of each with size 2000, with different means and variances as our real source representation \mathbf{s} . Specifically, $s_i \sim N(\boldsymbol{\mu}_i, \boldsymbol{\Sigma}_i), i = 0, \dots, 6$, where $\boldsymbol{\mu}_0 = [-0.5, -1], \boldsymbol{\mu}_1 = [2, 1], \boldsymbol{\mu}_2 = [5, 2], \boldsymbol{\mu}_3 = [1, 3], \boldsymbol{\mu}_4 = [-2, 1], \boldsymbol{\mu}_5 = [-3.5, 4], \boldsymbol{\mu}_6 = [-4, -1], \boldsymbol{\Sigma}_0 = [0.5, 0.5], \boldsymbol{\Sigma}_1 = [3, 1], \boldsymbol{\Sigma}_2 = [1, 2], \boldsymbol{\Sigma}_3 = [0.3, 2], \boldsymbol{\Sigma}_4 = [1, 0.2], \boldsymbol{\Sigma}_5 = [1, 1], \boldsymbol{\Sigma}_6 = [2, 0.3]$. Then we perform classical Hénon transformation $z_{(1)} = 1 - 1.4 \tilde{s}_{(1)}^2 + \tilde{s}_{(2)}, z_{(2)} = 0.3, \tilde{s}_{(1)}$ to generate the data in feature space.

D.2. Extreme-classification Toy Data

We sample 1000 groups of two-dimensional uncorrelated Gaussian with mean ranges uniformly sampled from range $(-4, 4)$ and standard deviation fixed to 0.1. Validation dataset is fixed with 20 samples per-class, and the sampler per class in training dataset varies with 5, 10, 20, 50, 75, 100, 150. The summary for extreme-classification is presented in Table S1.

Note that when the total number of categories is 10 with 20 samples per class, ERM has top-1 accuracy as high as 0.914, and the performance drops when the number of categories increasing. With 500 categories, the accuracy decreases to 0.005, and in the scenario where we presented in the main text with 1000 categories, ERM performs no better than random guessing.

Table S1. Validation Results for Extreme classification

METRIC	NLL			TOP 1			TOP5		
	ERM	ECRT W/O AUG	ECRT	ERM	ECRT W/O AUG	ECRT	ERM	ECRT W/O AUG	ECRT
5	6.9246	4.3884	3.7098	0.0015	0.0450	0.0760	0.0053	0.2275	0.3220
10	6.9242	4.0536	3.4752	0.0018	0.0638	0.0856	0.0060	0.2666	0.3549
20	6.9185	3.5405	3.3657	0.0016	0.0741	0.0877	0.0070	0.3126	0.3675
50	6.9240	3.3794	3.2957	0.0010	0.0834	0.0934	0.0045	0.3493	0.3835
75	6.9190	3.3499	3.2594	0.0020	0.0846	0.0939	0.0060	0.3571	0.3950
100	6.9182	3.3394	3.2675	0.0020	0.0834	0.0934	0.0053	0.3580	0.3918
150	6.9174	3.2731	3.2597	0.0011	0.0906	0.0984	0.0059	0.3777	0.4034

E. Real-world Data Experiments

E.1. Image Data Benchmarks

We summarized the image datasets in Table S2 and the network architectures used for respective datasets in Tables S3, S4, S5 and S6. The hyperparameters we used in these experiments are presented in S10. The results reported here are from our regularized non-parametric ECRT implementation, parametric ECRT implementation show a similar trend, with slightly improved performance (results now shown). We use 2 latent dims for MNIST and 32 latent dims for CIFAR100, iNaturalist and Tiny-Imagenet.

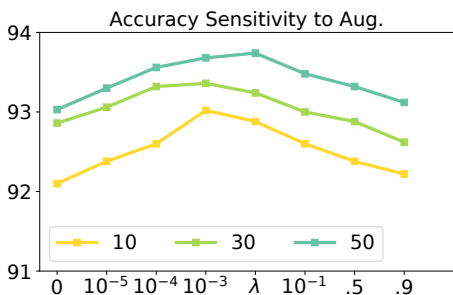


Figure S3. Sensitivity analysis (overall top 1 accuracy) of augmentation strength λ . Complementing Figure 11 in main text.

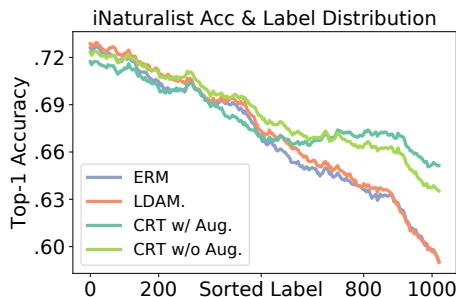


Figure S4. Class-conditional Top-1 accuracy curve for iNat2019. Complementing Figure 1 (F1 score). Note that ERM and LDAM show better accuracy for sample-rich majorities, but worse F1 scores. This evidences majority bias, that a predictor has a low specificity for data rich classes.

Preprocessing For iNaturalist dataset, we used pretrained Inception V3 to extract the features with dim=2048. For Tiny-Imagenet we finetuned the Resnet 18 to extract the features with dim = 512.

Baselines We used the ERM, LDAM¹, Focal², IW³, and VAT⁴ baseline implementations. For GAN we adopted the CGAN model with architecture shown in S9 and noise dimension listed in S11 for each dataset. We compared all the models with their own best performance after early stopping.

Discrepancy of baseline performance. We noticed that our implementation of baseline models, especially for the ERM baseline, yields results better than what’s reported in literature (LDAM in particular). Specifically, our results look better. After carefully compared our implementation to the LDAM codebase, we see that the discrepancy comes from the choice of optimizer. The use of vanilla SGD optimizer, as practiced in LDAM, results in degraded performance of baseline, and consequently a larger performance gap compared to strong solutions.

Majority bias. In Figure S4, we give the top-1 accuracy wrt different minority size on the iNaturalist dataset. This figure is complementary to the F1-label frequency plot given in Figure 14 from the main text. While the improvement at the tail part are strong under both metrics, we see clear evidence of majority bias in the Top-1 accuracy plot. ERM and LDAM show better performance in accuracy for the sample abundant majority regime, but severe performance drop in the sample deficient minority regime. This is because ERM and alike finds it more rewarding to favor the majorities during inference, which gives better sensitivity but much worse specificity for the majority samples, and consistently hurting the performance for minorities.

E.2. Language Data Benchmark

Dataset and preprocessing. In this experiment, have used the arXiv dataset hosted on Kaggle⁵. We use the pretrained BERT model from the transformers package⁶ to extract sentence features. Specifically, we applied the SciBERT model (allenai/scibert.scivocab_uncased) [1], and used the BERT default 768-dimensional sentence embedding for each abstract. The training set includes 160k data, where class labels with more than 5k samples are identified as majority

¹<https://github.com/kaidic/LDAM-DRW>

²<https://github.com/artemavrin/focal-loss>

³<https://github.com/idiap/importance-sampling>

⁴<https://github.com/lyakaap/VAT-pytorch>

⁵<https://www.kaggle.com/Cornell-University/arxiv>

⁶<https://github.com/huggingface/transformers>

classes, with the rest assigned to minority label classes. All label classes with less than 20 samples have been excluded from our analysis. This gives us a total of 14 majority classes and 138 minority classes.

Setup. Different from the image benchmarks, the `arXiv` data is a multi-label prediction task. Each abstract is associated with at least one, possibly multiple labels, and we make binary classifications for each label class. In the training of GCL model, we allow samples with multiple labels to be reused by different classes, as each constructs a valid source IC distribution under our hypothesis. Only standard ECRT is considered in this experiment. We set the source space dimension to 64 and use the network architecture described in Table S7.

Evaluation. The accuracy reported for this experiment is defined as follows: say a sample is associated with k -labels, then we compared the top- k predicted labels to the true labels, and report the averaged accuracy for this sample. Like previous experiments, we target a balanced evaluation set. However, getting a perfectly balanced evaluation set is impossible here, as samples are associated with multiple labels. We extracted a nearly-balanced evaluation set including 847 samples, where each label has 10 to 50 counts. Most of classes have 10-15 samples in our nearly-balanced evaluation set.

Table S2. Summary of datasets

NAME	DIM	TRAIN (MAJORITY)	TRAIN (MINORITY)	VALIDATION
MNIST	(28×28)	$6000 \times (1 \text{ OR } 5)$ (CLS)	$1200 \times (1 \text{ OR } 5)$ (CLS)	1000×10 (CLS)
CIFAR	$(32 \times 32 \times 3)$	500×50 (CLS)	500×50 (CLS)	100×100 (CLS)
INAT	$(\text{NONE} \times \text{NONE} \times 3)$	$(\geq 120) \times 725$ (CLS)	$(< 120) \times 285$ (CLS)	3×1010 (CLS)
TINY	$(64 \times 64 \times 3)$	450×100 (CLS)	45×100 (CLS)	50×200 (CLS)
ARXIV	<i>(None)</i>	$(> 5000) \times 14$ (CLS)	$(< 5000) \times 138$ (CLS)	12×152 (CLS)

Table S3. MNIST experiment network architecture.

NETWORK	ARCHITECTURE
ENCODER	FC(UNIT=32)+RELU + FC(UNIT=32)+RELU + FC(UNIT=2)
DECODER	FC(UNIT=32)+RELU + FC(UNIT=32)+RELU + FC(UNIT=10)
FLOW	MAF($n_{blocks} = 4$, $hidden_{size} = 128$, $n_{hidden} = 2$).

Table S4. Cifar100 experiment network architecture.

NETWORK	ARCHITECTURE
ENCODER	RESNET18 ^a + FC(UNIT=32)
DECODER	FC(UNIT=256)+RELU FC(UNIT=100)
FLOW	MAF($n_{blocks} = 4$, $hidden_{size} = 128$, $n_{hidden} = 2$).

^aResnet 18 without last layer

TABLE S5. INATURALIST EXPERIMENT NETWORK ARCHITECTURE.

NETWORK	ARCHITECTURE
PRETRAIN	INCEPTION(V3)
ENCODER	FC(UNIT=1024)+RELU +DROPOUT(0.1) + FC(UNIT=512)+RELU +DROPOUT(0.1) + FC(UNIT=32)
DECODER	FC(UNIT=32)+RELU +DROPOUT(0.1) + FC(UNIT=512)+RELU +DROPOUT(0.1) + FC(UNIT=1010)
FLOW	MAF($n_{blocks} = 4$, $hidden_{size} = 128$, $n_{hidden} = 2$).

TABLE S6. TINY IMAGENET EXPERIMENT NETWORK ARCHITECTURE.

NETWORK	ARCHITECTURE
PRETRAIN	RESNET18
ENCODER	FC(UNIT=1024)+RELU +DROPOUT(0.1) + FC(UNIT=512)+RELU +DROPOUT(0.1) + FC(UNIT=32)
DECODER	FC(UNIT=512)+RELU +DROPOUT(0.1) + FC(UNIT=200)
FLOW	MAF($n_{blocks} = 4$, $hidden_{size} = 128$, $n_{hidden} = 2$).

TABLE S7. ARXIV EXPERIMENT NETWORK ARCHITECTURE.

NETWORK	ARCHITECTURE
PRETRAIN	BERT
ENCODER	FC(UNIT=1024)+RELU +DROPOUT(0.1) + FC(UNIT=512)+RELU +DROPOUT(0.1) + FC(UNIT=64)
DECODER	FC(UNIT=64)+RELU +DROPOUT(0.1) + FC(UNIT=512)+RELU +DROPOUT(0.1) + FC(UNIT=152)
FLOW	MAF($n_{blocks} = 4$, $hidden_{size} = 128$, $n_{hidden} = 2$).

Table S8. MNIST results with different numbers of minority categories

# MINORITY LABEL	1		5	
	NLL	TOP 1	NLL	TOP 1
ERM	0.342	0.933	0.390	0.904
LDAM	1.6737	0.9609	1.50	0.940
ECRT	0.186	0.972	0.257	0.950

TABLE S9. GAN NETWORK ARCHITECTURE.

NETWORK	ARCHITECTURE
GENERATOR	FC(UNIT=256) +LEAKYRELU + FC(UNIT=256)+LEAKYRELU +FC(UNIT=LATENT _{dim})
DISCRIMINATOR	FC(UNIT=256) +LEAKYRELU +DROPOUT(0.1) + FC(UNIT=256)+LEAKYRELU +DROPOUT(0.1) +FC(UNIT=1)+SIGMOID

TABLE S10. HYPERPARAMETER OF DATASETS (ECRT)

NAME	REG WEIGHT	AUG STRENGTH
MNIST	1E-2	1E-3
CIFAR	1E-2	1E-3
INAT	5E-3	1E-3
TINY	1E-3	1E-3
ARXIV	1E-2	1E-2

TABLE S11. HYPERPARAMETER OF DATASETS (GAN)

NAME	NOISE DIM
MNIST	32
CIFAR	64
INAT	128
TINY	128
ARXIV	64

References

- [1] Iz Beltagy, Kyle Lo, and Arman Cohan. SciBERT: A pretrained language model for scientific text. In *EMNLP. ACL*, 2019. 6
- [2] Ricky TQ Chen, Yulia Rubanova, Jesse Bettencourt, and David K Duvenaud. Neural ordinary differential equations. In *NeurIPS*, 2018. 4
- [3] Qing Guo, Junya Chen, Dong Wang, Yuewei Yang, Xinwei Deng, Fan Li, Lawrence Carin, and Chenyang Tao. Tight mutual information estimation with contrastive Fenchel-Legendre optimization, 2021. [Available online; accessed 28-May-2021]. 3
- [4] Aapo Hyvarinen, Hiroaki Sasaki, and Richard Turner. Nonlinear ica using auxiliary variables and generalized contrastive learning. In *AISTATS*, pages 859–868, 2019. 2
- [5] Ker-Chau Li. Sliced inverse regression for dimension reduction. *Journal of the American Statistical Association*, 86(414):316–327, 1991. 4
- [6] George Papamakarios, Theo Pavlakou, and Iain Murray. Masked autoregressive flow for density estimation. In *NIPS*, 2017. 4
- [7] Danilo Jimenez Rezende and Shakir Mohamed. Variational inference with normalizing flows. In *ICML*, 2015. 4
- [8] Joshua Robinson, Stefanie Jegelka, and Suvrit Sra. Strength from weakness: Fast learning using weak supervision. In *ICML*, 2020. 3
- [9] Takeshi Teshima, Issei Sato, and Masashi Sugiyama. Few-shot domain adaptation by causal mechanism transfer. In *ICML*, 2020. 2